ACS APPLIED MATERIALS & INTERFACES
Research Article
www.acsami.org

Negative Differential Resistance Behavior and Memory Effect in Laterally Bridged ZnO Nanorods Grown by Hydrothermal Method

Ming-Yueh Chuang,[†] Ying-Chih Chen,[†] Yan-Kuin Su,*[,†,‡] Chih-Hung Hsiao,[†] Chien-Sheng Huang,[§] Jeng-Je Tsai,[§] and Hsin-Chieh Yu[†]

[†]Institute of Microelectronics and Advanced Optoelectronic Technology Center, National Cheng Kung University, Tainan 701, Taiwan

[‡]Department of Electrical Engineering, Kun Shan University, Tainan 710, Taiwan

[§]Department of Optoelectronics Engineering, National Yunlin University of Science and Technology, Douliou 64002, Taiwan

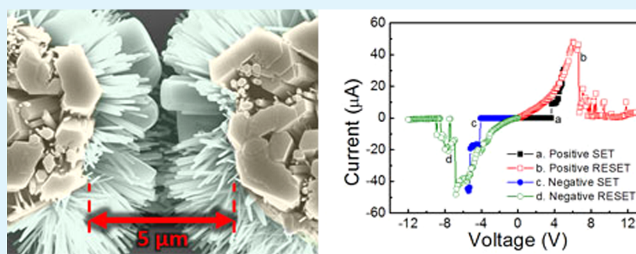

ABSTRACT: A novel memory device based on laterally bridged ZnO nanorods (NRs) in the opposite direction was fabricated by the hydrothermal growth method and characterized. The electrodes were defined by a simple photolithography method. This method has lower cost, simpler process, and higher reliability than the traditional focused ion beam lithography method. For the first time, the negative differential resistance and bistable unipolar resistive switching (RS) behavior in the current−voltage curve was observed at room temperature. The memory device is stable and rewritable; it has an ultra-low current level of about 1×10^{-13} A in the high resistance state; and it is nonvolatile with an on−off current ratio of up to 1.56×10^6. Moreover, its peak-to-valley current ratio of negative differential resistance behavior is greater than 1.76×10^2. The negative differential resistance and RS behavior of this device may be related to the boundaries between the opposite bridged ZnO NRs. Specifically, the RS behavior found in ZnO NR devices with a remarkable isolated boundary at the NR/NR interface was discussed for the first time. The memory mechanism of laterally bridged ZnO NR-based devices has not been discussed in the literature yet. In this work, results show that laterally bridged ZnO NR-based devices may have next-generation resistive memories and nanoelectronic applications.

KEYWORDS: *laterally bridged, ZnO nanorod, hydrothermal growth, resistive random access memory, unipolar*

1. INTRODUCTION

As conventional flash memories approach their technological and physical limits in scaling reduction, resistive random access memory (ReRAM) has been attracting much attention because of its many advantages, such as simple structure, high density integration, high operational speed, low-power consumption, and potential for the replacement of flash memories in next-generation nonvolatile memories.[1−3] RS behaviors have been extensively investigated in various materials, such as binary transition metal oxides,[4−7] perovskite oxides,[8,9] organic compounds,[10−12] and graphene oxide,[13] among others. To explain the RS phenomenon, researchers have proposed many theoretical models. The most believable explanation is the formation and rupture of conductive filaments in the insulator.[2] Other plausible models, such as field-assisted drift/diffusion of charged ions, trap-controlled space-charge-limited current, Frenkel−Poole emission, and Schottky barriers, have been widely proposed.[14−16]

One-dimensional (1D) ZnO nanorods (NRs) have attracted much attention recently as potential candidates for nanoscale devices.[17] The peculiar physical properties in confined dimensions of ZnO NR-based ReRAM enable it to have such characteristics as ultralow leakage current in the high resistive state (HRS), large memory window, and low switching voltage. Furthermore, ZnO NR-based ReRAM has the potential to break through the present lithography limitation and increase the area density of memory cells. So far, the origins of these behaviors in laterally bridged ZnO NR-based ReRAM remain unclear. Therefore, investigating and studying the electric property in nano-scale devices are necessary to advance toward next-generation memory devices. High-quality vertical ZnO NR arrays are grown by several approaches, such as the gas transport technique,[18,19] metal−organic chemical vapor deposition,[20] and hydrothermal method.[21−23] ZnO generally has a strong leaning toward self-assembled growth. This important tendency has led to the great interest in growing particular nanostructures by controlling growth parameters for vertical optoelectronic applications. Vertical alignment, selective growth, and controlled morphology of NRs have recently stimulated interest in 1D nanostructure applications. However, direct contact between the top and bottom electrodes may cause a short circuit problem if the top electrode is fabricated

Received: November 1, 2013
Accepted: March 13, 2014
Published: March 13, 2014

ACS Publications © 2014 American Chemical Society

on a ZnO NR with a low packing density.[24] By contrast, the fabrication of lateral ZnO NR-based devices is much simpler. Moreover, the concept of lateral structure not only solves the short circuit problem but also realizes integrated submicrometer/nanoscale devices on a planar substrate. Currently, these 1D ZnO NR-based devices can be achieved by randomly dispersing a single ZnO NR onto pre-fabricated electrodes,[25,26] using electron-beam lithography,[27] or using focused-ion-beam deposition[28] to individually delineate the electrical contacts. The general drawbacks of the reported techniques are that they require complex and time-consuming processing steps and restrict the realistic mass fabrication and large-scale manufacturing of lateral ZnO NR-based devices.

So far, the RS behaviors have been widely reported in ZnO thin films[29,30] but few in ZnO NRs. Chang et al. investigate the RS characteristics of vertically aligned ZnO NR layers prepared by hydrothermal growth (HTG) method.[31] The Pt/ZnO NR layer/ITO device exhibit reversible and steady bipolar RS behavior. Chiang's paper[32] reports a single-ZnO-nanowire memory device based on unipolar RS behavior is demonstrated for the first time. The memory device is stable, rewritable, and nonvolatile with on-and-off ratio up to 7.7×10^5. Compared with ZnO thin film-based memory devices, a 1D nanostructure can provide a localized conducting filament in devices that allow RS operation with a narrow dispersion of operational parameters.[24] Besides, the investigation of RS behavior in confined dimensional systems may bring new insights into the underlying mechanism.[33]

In this study, we successfully fabricated and characterized a new kind of ReRAM device with a bridged ZnO NR structure synthesized through HTG at low temperature under 90 °C. The device fabrication used a simple, stable, and reliable method without focused ion beam lithography or a randomly dispersed process. Field-emission scanning electron microscopy (FE-SEM) and micro photoluminescence (micro-PL) spectroscopy indicated that oxygen vacancies at the boundaries of ZnO NR/NR were observed and might play a role in the RS behavior. This paper opens the possibility of developing laterally bridged ZnO NR-based ReRAM.

2. EXPERIMENTAL DETAILS

Figure 1 shows a schematic view of the memory device based on laterally bridged ZnO NRs in the opposite direction. The detailed procedure is described as follows. An 80 nm thick SiO_2 dielectric layer was first deposited on a Si substrate by electron-beam evaporation. Then, a 2 μm thick Au metal was defined by standard photolithography to serve as a catalyst and metal contact. The patterned substrates were immersed in an HTG solution of 25.2 mM $Zn(NO_3)_2 \cdot 4H_2O$ and 33.4 mM $C_6H_{12}N_4$ at 90 °C for 1.5 h. Afterwards, the samples were removed from the solution, rinsed in deionized water, and dried thoroughly. Finally, the as-grown ZnO NRs were annealed in vacuum under a pressure of 5×10^{-3} Torr using the rapid thermal process system. Samples were heated from room temperature to 600 °C for 10 min at a heating rate of 60 °C/min and then cooled to room temperature. The annealing process is mainly used to improve the contact between ZnO NRs and Au electrodes, and the contact resistance can be further reduced by annealing process at 600 °C.[34] The morphology and distribution of lateral ZnO NRs were characterized by FE-SEM (Hitachi SU8000). Micro-PL spectroscopy was used at room temperature using a 325 nm He−Cd laser to examine the oxygen-related defects. The current−voltage (I−V) characteristics of all memory devices were measured by a Keithley 2400 source meter. The electrical analyses were carried out in a nitrogen-filled glove box system at room temperature.

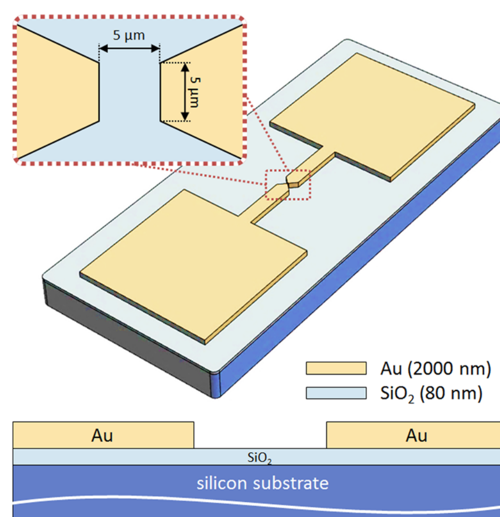

Figure 1. Schematic illustration of the memory device based on laterally bridged ZnO NRs in the opposite direction. Prior to the growth of lateral ZnO NRs, the Au metal is defined by photolithography.

3. RESULTS AND DISCUSSION

Figure 2 shows the typical FE-SEM images of ZnO NRs laterally grown across the gap between the electrodes, which formed laterally bridged ZnO NRs and provided a carrier transporting path. The average diameter and length of ZnO NRs were 0.15 and 2.6 μm, respectively. The two-terminal electrical measurement of laterally bridged ZnO NR-based memory devices was conducted across a pair of Au electrodes. During the first applied external voltage sweeping from 0 to 10 V, the unusual-forming process was achieved by applying a high voltage of approximately +9.5 V with a current of 3 mA, as shown in the insert of Figure 3a. Moreover, there was no RS behavior could be observed from the I−V curves that measured before unusual-forming as shown in Figure 3a. The unusual-forming process is similar to a soft breakdown, and it increases the defect states located at the NR/NR boundaries. After the unusual-forming process, the state of the device became the HRS in the order of $\sim 1 \times 10^{10}$ Ω. As shown in Figure 3b), in both positive and negative bias sweeping directions, a symmetric nonlinear I−V characteristic and unipolar RS behavior were observed. Moreover, the bistable RS behavior was reversible and steady.

To understand the switching property, the I−V curves were redrawn in a semi-logarithmic plot with a more detailed description, as shown in Figure 3c. The sequence for measurement is as follows: (1) 0−2 V, to confirm the HRS; (2) 0−5 V, the SET process; (3) 0−2 V, to confirm the LRS; (4) 0−13 V, the RESET process; and (5) 0−2 V: to confirm the HRS. The SET voltage (V_{SET}) and RESET voltage (V_{RESET}) took place at 3.6 and 6.6 V, respectively. V_{SET} was smaller than V_{RESET} for laterally bridged ZnO NR-based memory cells, which is uncommon in typical unipolar RS behaviors. The analogous RS phenomenon observed from a single-ZnO-nanowire memory cell was reported by Chiang et al.[32] The characteristic of $V_{SET} < V_{RESET}$ is anticipated to prevent burn-off and breakdown directly caused by the large Joule heating generated during the RESET process. The resistance state can be determined using the reading voltage (V_{READ}) ranging from 0 to V_{SET} without affecting the data stored in a memory cell. In

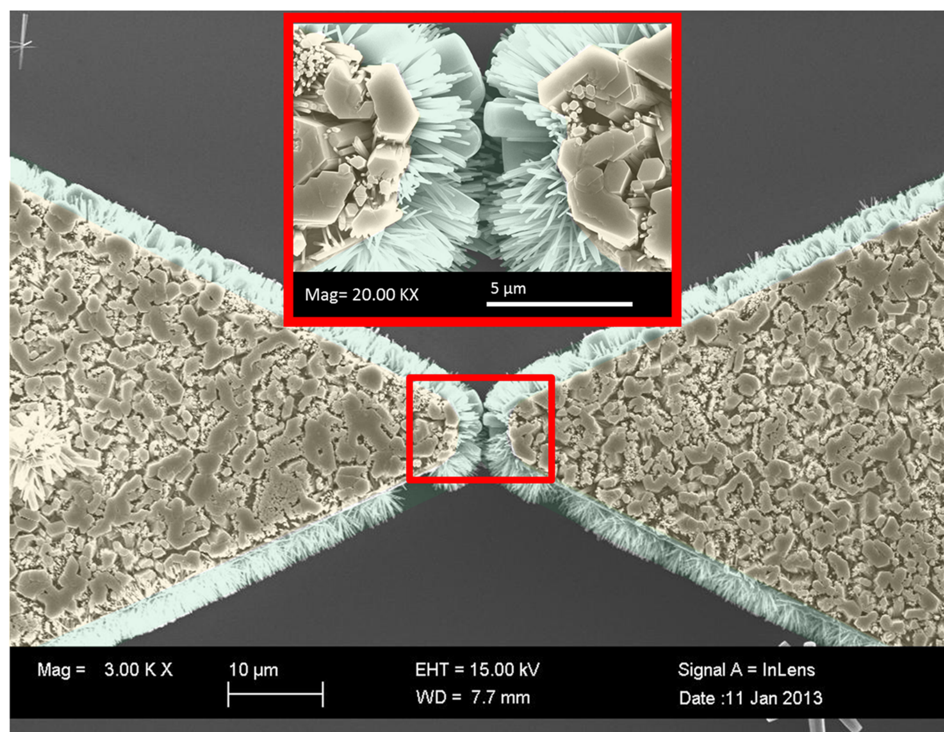

Figure 2. Typical FE-SEM plane-view images of laterally bridged ZnO NRs. The ZnO NRs were grown in an HTG solution of 25.2 mM $Zn(NO_3)_2 \cdot 4H_2O$ and 33.4 mM $C_6H_{12}N_4$ at 90 °C for 8 h. As-grown ZnO NRs were annealed in a vacuum under a pressure of 5×10^{-3} Torr using a tube furnace.

this paper, the V_{READ} is set to 500 mV. The memory window defined by the two resistance states

$$(R_{off} - R_{on})/R_{on} \cong R_{off}/R_{on} \quad (1)$$

is more than 1×10^6 at a reading voltage of 0.5 V from Figure 3b. The laterally bridged ZnO NR-based memory cell easily distinguished the stored data between "1" and "0" because of the high memory window of the present device.

To understand the unusual-forming process of laterally bridged ZnO NR-based memory devices, the room temperature (RT) micro-PL spectra were measured by the He−Cd laser at 325 nm to examine the defect states in as-synthesized and unusual-formed ZnO NRs, as shown in Figure 4. The micro-PL laser spot was focused on the center of laterally bridged ZnO NRs, and the diameter of the laser spot was about 3 μm, as shown in the insert of Figure 4. The intensity of the defect state emission of ZnO NRs, such as monovalent interstitial zinc (Zn_i^+), zinc vacancy (V_{Zn}), and monovalent vacancies of oxygen (V_O^+), increases after the unusual-forming process.[35,36] These results indicate that the unusual-forming process not only increases the density of defect states but also the number of zinc and oxygen vacancy sites. These defect states play an important role in charge trapping. The trapped charge may be collected at the NR/NR boundary. Negative charges are trapped at the interface of NR/NR boundary, where energy band bending occurs and forms a back-to-back Schottky barrier. According to previous reports,[37,38] energy band bending at the interface/boundary results in a higher Schottky barrier. The barrier height (φ_B) can be obtained by solving the Poisson's equation including the interface charge

$$\varphi_B = \frac{qN_{IS}^2}{2N_d\varepsilon_r\varepsilon_0} \quad (2)$$

where N_{IS} is the density of trapped charge in the interface, ε_r is the relative permittivity, ε_0 is the permittivity of free space, and q is the elementary charge. The result of this equilibrium is that the interface-trapped electrons act as a sheet of negative charge at the boundary, leaving behind a layer of positively charged donor sites on either side of the boundary, and create an electrostatic field with a barrier at the boundary. When the number of charge trapping increases, the barrier height increases.[38] Figure 5 shows the schematic energy band diagram of the Schottky barrier when the applied voltage is zero. The barrier height of the device after the unusual-forming process ($e\varphi_2$) is higher than that of the one as-synthesized ($e\varphi_1$) because of more trapped charges at the interface. The results indicate that unusual-forming process in this structure can lower the current level and open the memory window of the devices.

To confirm this phenomenon, the NRs were grown at a growth time of 8 h and 10 h for samples 1 and 2, respectively. The average length of ZnO NRs was 2.6 μm and 3.2 μm for sample 1 and 2, respectively. Because of the gap between electrodes was 5 μm, the bridged structure of sample 1 was almost cohered with about 200 nm overlapping and that of sample 2 was fully cohered with 1.2 μm overlapping. After the unusual-forming process, the $I-V$ curves of samples 1 and 2 exhibited symmetric and asymmetric curves, respectively, as shown in Figure 6a. Interestingly, the significant RS behavior was discovered only in sample 1. Panels b and c in Figure 6 show the resistance in each region for samples 1 and 2, respectively. For sample 1, the boundary resistance (R_B) was larger than the contact resistance (R_c). Thus, the Joule heating accumulated at the boundary and damaged it. For sample 2, the R_B was smaller than the R_c. The damaged interface occurred at the contact between metal and ZnO NRs. Therefore, sample 1

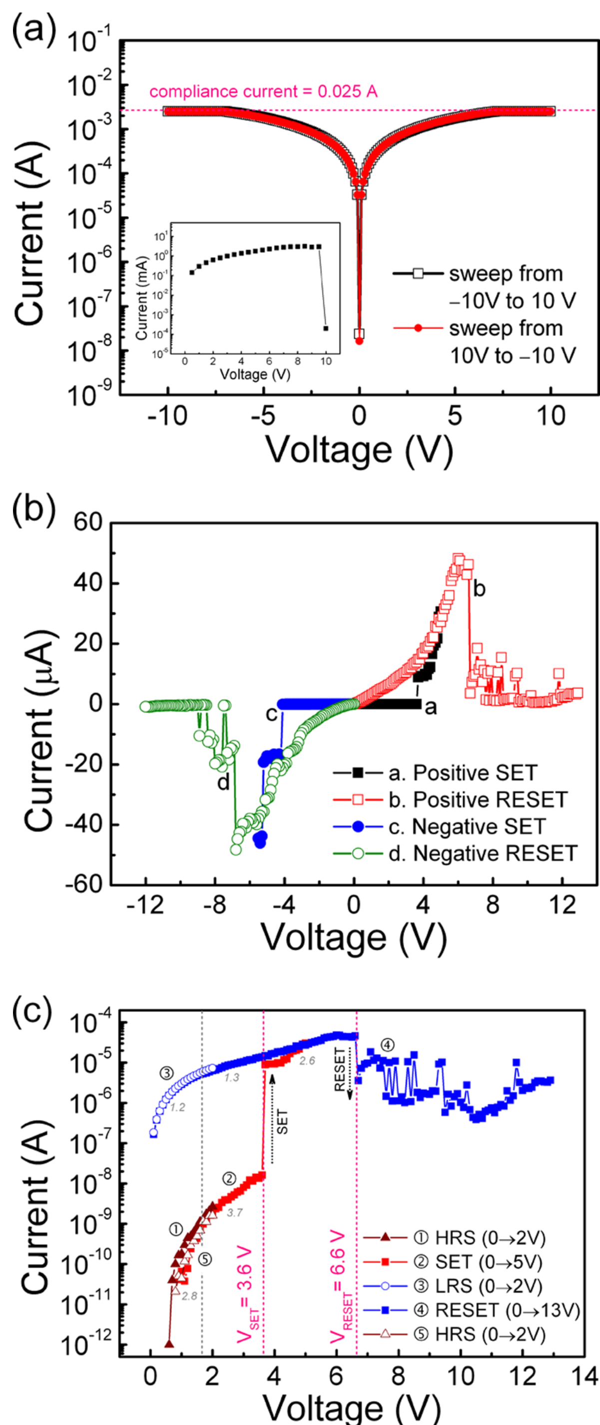

Figure 3. (a) $I-V$ characteristics before unusual-forming process performed by voltage sweepings with compliance current of 0.025A. (Inset) The unusual-forming process occurred at 9.5 V. (b) Bistable and unipolar RS characteristics of a laterally bridged ZnO NR-based memory device after the unusual-forming process. Curves a, b, c, and d denote the positive SET, positive RESET, negative SET, and negative RESET processes, respectively. (c) Unipolar RS $I-V$ curve in the semi-logarithmic plot of a laterally bridged ZnO NR-based memory device in the voltage-sweeping mode. The SET and RESET voltages are 3.6 and 6.6 V, respectively.

exhibited the symmetric $I-V$ characteristic and unipolar RS behavior. On the basis of these results, the unusual-forming process of the device may be attributed to the formation of more defect states, and the defect states may be produced at the boundary of the opposite bridged NRs. The current density of the fabricated memory cell measured from the insert in Figure 3a approached 3×10^4 A cm^{-2}. This current density is large enough to induce a thermally assisted electromigration[39,40] of oxygen vacancies at the NR/NR interfaces caused by the accompanying Joule heating effect.[41,42] According to previous literature, the RS behavior may be highly related to the oxygen vacancies and/or zinc interstitials confined on the surface of ZnO NRs.[31,43,44]

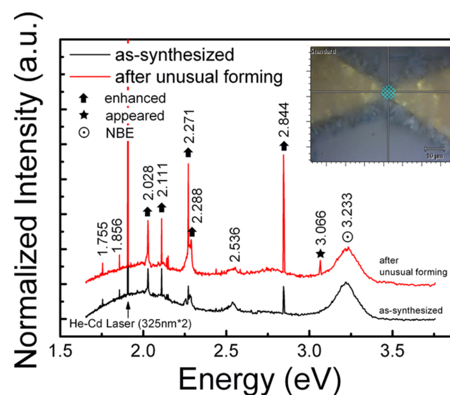

Figure 4. RT micro-PL spectra of as-synthesized and after unusual-forming laterally bridged ZnO NRs. (Inset) Location of the laser spot.

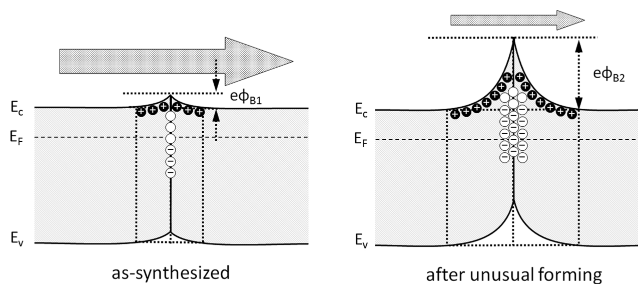

Figure 5. Band structure diagram of a double Schottky barrier in equilibrium for a ZnO grain boundary with the two NRs in opposite directions, where E_c, E_F, and E_v are the bottom of the conduction band, Fermi level, and top of the valence band, respectively. (a) Scheme of the band structure without unusual-forming (as-synthesized). (b) Schematic presentation after the unusual-forming process. Note the representation of a higher barrier height ($e\varphi_{B2} > e\varphi_{B1}$) of the junction after unusual-forming. The trapped electron density is higher than the as-synthesized one because of the large number of defect states (interfacial state) created by the unusual-forming process (i.e., Zn_i^+, V_{Zn}, and V_O^+).

Figure 6d shows the schematic presentation of the regions of filament generation and ohmic conduction. The defects concentrated at the boundaries of NR/NR interfaces. The equivalent thickness of memory cell was much less than the total length of laterally bridged ZnO NR. The formation and rupture of conductive filaments occurred at the boundaries of NR/NR interfaces resulting from the high density of accumulated defects. Accordingly, the V_{SET} and V_{RESET} of fabricated memory cell were significantly smaller than the values reported by Chiang et al.[32]

To clarify the conduction and switching mechanisms of the memory cell, the previous $I-V$ characteristics were re-drawn in a double logarithmic scale, as shown in Figure 7. The $I-V$ curve in LRS showed a linear behavior under low voltage ($<V_{SET} \approx$ 3.6 V). The conduction mechanisms clearly showed an ohmic behavior because the curve of the logI−logV was linearly fitted

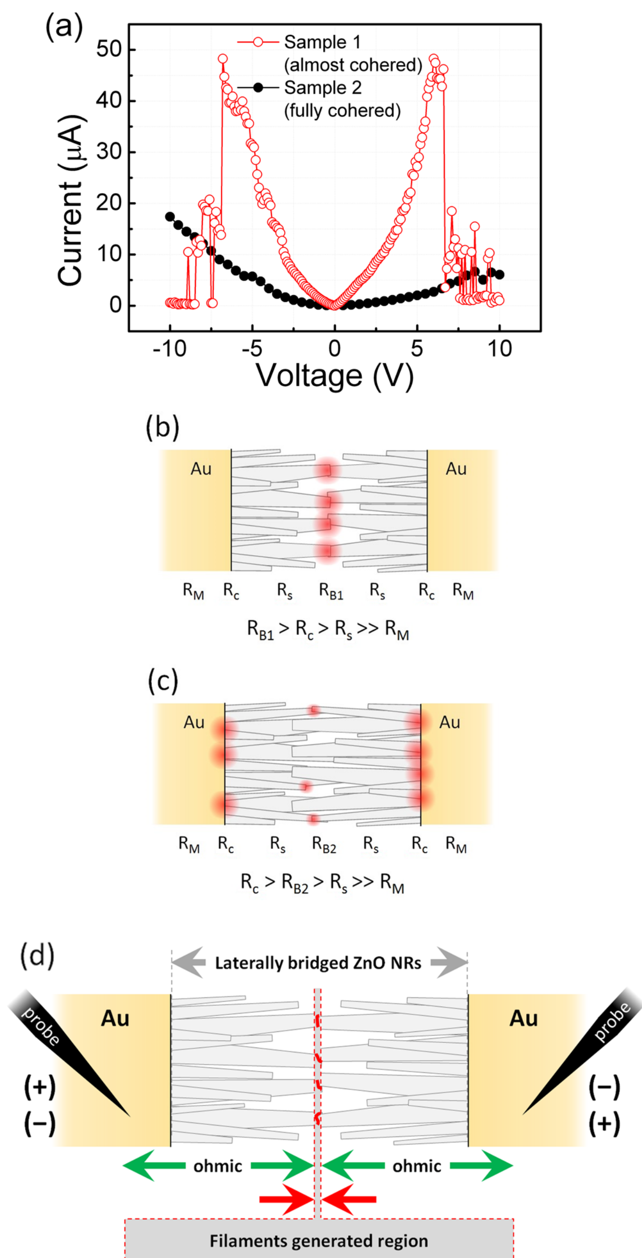

Figure 6. (a) $I-V$ characteristic of samples 1 and 2 after the unusual-forming process. The schematic diagram is shown as (b) sample 1 (almost cohered) and (c) sample 2 (fully cohered), where R_B, R_M, R_C, and R_S are the resistance of the NR/NR boundary, Au, contact, and ZnO NR, respectively. The red spots indicate the damaged area by the unusual-forming process because of the generated Joule heating. (d) Schematic presentation of the filaments in the generated region and the ohmic conduction region.

well with a slope of about 1.22, which could be considered to correspond to the formation of conductive filaments at the boundaries of NR/NR interfaces during the SET process.[45] Then, at the voltage V_{SET} (3.6 V), the current increased slowly and the slope reached about 2.44. The charge transport behavior at the NR/NR boundaries can be explained by the one-hole carrier injected trap-controlled space-charge-limited conduction mechanism. However, an entirely different current mechanism might have dominated in HRS. The fitting of the currents was approximately 4.47. The number of carriers injected into the boundaries of the NR/NR interfaces was

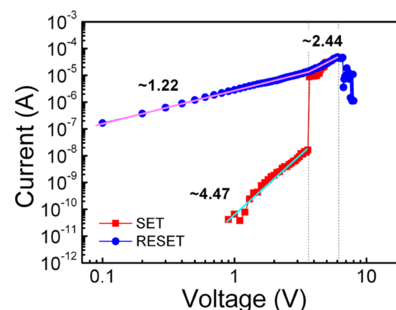

Figure 7. Experimental $I-V$ data and fitted data in the RESET and SET processes and the corresponding slopes for each portion.

significantly higher in this voltage range than in any other range, and the $I-V$ data consequently followed a typical space-charge-limited current with a trap model, which is known as the trapped charge-limit-current mechanism.[46,47] The large slope value of the fitting line indicates that the traps in the boundaries of the NR/NR interfaces are exponentially distributed over energy in the ZnO band gap.

Figure 8a shows that the memory window remained beyond 11 times during cycling, and that the memory cell showed little

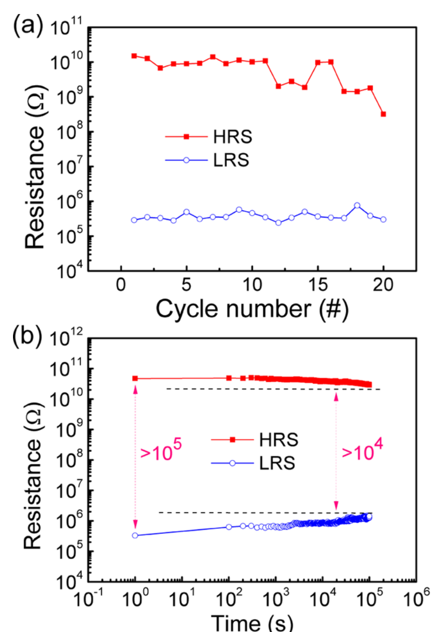

Figure 8. (a) Endurance performance of the fabricated device. Application of +5 V 500 ms to switch the memory state to ON state and +10 V 500 ms pulse to switch it back to the OFF state. (b) Retention performance of laterally bridged ZnO NR-based memory devices in $1 \times 10_5$ s under 0.5 V read voltage. The resistances in the HRS and LRS only show a slight change in more than 1×10^5 s under room temperature.

degradation after 20 repeated sweep cycles. The endurance measurements that ensured the switching between on and off states were highly controllable, reversible, and reproducible. After the device was switched on or off, no electrical power was needed to maintain the resistance within the given state. The retention performance was also measured, as shown in Figure 8b. Clearly, the resistance in both states was demonstrated to remain for 1×10^5 s, and the on−off ratio was $>1 \times 10^4$. The excellent retention properties of fabricated memory cells show

dx.doi.org/10.1021/am404875s | ACS Appl. Mater. Interfaces 2014, 6, 5432−5438

that laterally bridged ZnO NRs are the potential structures for ReRAM application.

4. CONCLUSION

In summary, we developed a laterally bridged ZnO NR-based memory device with unique and excellent memory characteristics using a simple fabrication process. A preliminary investigation and thorough discussion of isolated boundaries were performed for the first time. The equivalent thickness of the memory cell was much less than the total length of a laterally bridged ZnO NR. The formation and rupture of conductive filaments occurred at the boundaries of the NR/NR interfaces resulting from the high density of accumulated defects. The laterally bridged ZnO NR-based memory is stable, rewritable, and nonvolatile with on−off current ratio higher than 1×10^6 and long retention up to 1.56×10^6 s. This finding confirms that the laterally bridged ZnO NR-based device is a potential candidate for application in next-generation nonvolatile memory.

■ AUTHOR INFORMATION

Corresponding Author

*E-mail: yksu@mail.ncku.edu.tw.

Notes

The authors declare no competing financial interest.

■ ACKNOWLEDGMENTS

The authors thank the Center for Micro/Nano Science and Technology of National Cheng Kung University for the assistance in device characterization. This study was financially supported by the Advanced Optoelectronic Technology Center, National Cheng Kung University, under the projects of the Ministry of Education and the National Science Council (NSC 102-2221-E-006-211-/102-2811-E-006-039-) of Taiwan, R.O.C.

■ ABBREVIATIONS

NRs, nanorods
RS, resistive switching
ReRAM, resistive random access memory
1D, one-dimensional
LRS, low resistive state
HRS, high resistive state
HTG, hydrothermal growth
FE-SEM, field-emission scanning electron microscopy
micro-PL, micro photoluminescence
I−*V*, current−voltage
RT, room temperature

■ REFERENCES

(1) Asamitsu, A.; Tomioka, Y.; Kuwahara, H.; Tokura, Y. Current Switching of Resistive States in Magnetoresistive Manganites. *Nature* **1997**, *388*, 50−52.

(2) Waser, R.; Aono, M. Nanoionics-Based Resistive Switching Memories. *Nat. Mater.* **2007**, *6*, 833−840.

(3) Moreno, C.; Munuera, C.; Valencia, S.; Kronast, F.; Obradors, X.; Ocal, C. Reversible Resistive Switching and Multilevel Recording in $La_{0.7}Sr_{0.3}MnO_3$ Thin Films for Low Cost Nonvolatile Memories. *Nano Lett.* **2010**, *10*, 3828−3835.

(4) Ahn, S. E.; Lee, M. J.; Park, Y.; Kang, B. S.; Lee, C. B.; Kim, K. H.; Seo, S.; Suh, D. S.; Kim, D. C.; Hur, J.; Xianyu, W.; Stefanovich, G.; Yin, H.; Yoo, I. K.; Lee, J. H.; Park, J. B.; Baek, I. G.; Park, B. H. Write Current Reduction in Transition Metal Oxide Based Resistance-Change Memory. *Adv. Mater.* **2008**, *20*, 924−928.

(5) Rohde, C.; Choi, B. J.; Jeong, D. S.; Choi, S.; Zhao, J. S.; Hwang, C. S. Identification of a Determining Parameter for Resistive Switching of TiO_2 Thin Films. *Appl. Phys. Lett.* **2005**, *86*, 262907−3.

(6) Yang, J. J.; Pickett, M. D.; Li, X.; Ohlberg, D. A. A.; Stewart, D. R.; Williams, R. S. Memristive Switching Mechanism for Metal/Oxide/Metal Nanodevices. *Nat. Nanotechnol.* **2008**, *3*, 429−433.

(7) Fujiwara, K.; Nemoto, T.; Rozenberg, M. J.; Nakamura, Y.; Takagi, H. Resistance Switching and Formation of a Conductive Bridge in Metal/Binary Oxide/Metal Structure for Memory Devices. *Jpn. J. Appl. Phys.* **2008**, *47*, 6266−6271.

(8) Jung, K.; Seo, H.; Kim, Y.; Im, H.; Hong, J.; Park, J. W.; Lee, J. K. Temperature Dependence of High- and Low-Resistance Bistable States in Polycrystalline NiO Films. *Appl. Phys. Lett.* **2007**, *90*, 052104−3.

(9) Szot, K.; Speier, W.; Carius, R.; Zastrow, U.; Beyer, W. Localized Metallic Conductivity and Self-Healing during Thermal Reduction of $SrTiO_3$. *Phys. Rev. Lett.* **2002**, *88*, 075508−4.

(10) Scott, J. C.; Bozano, L. D. Nonvolatile Memory Elements Based on Organic Materials. *Adv. Mater.* **2007**, *19*, 1452−1463.

(11) Chen, Y. C.; Su, Y. K.; Yu, H. C.; Huang, C. Y.; Huang, T. S. Nonvolatile Memory Characteristics of Organic Thin Film Transistors Using Poly(2-hydroxyethyl methacrylate)-Based Polymer Multilayer Dielectric. *Appl. Phys. Lett.* **2011**, *99*, 143308−3.

(12) Yu, H. C.; Chen, Y. C.; Huang, C. Y.; Su, Y. K. Investigation of Nonvolatile Memory Effect of Organic Thin-Film Transistors with Triple Dielectric Layers. *Appl. Phys. Expr.* **2012**, *5*, 034101−3.

(13) Khurana, G.; Misra, P.; Katiyar, R. S. Forming Free Resistive Switching in Graphene Oxide Thin Film for Thermally Stable Nonvolatile Memory Applications. *J. Appl. Phys.* **2013**, *114*, 124508−6.

(14) Odagawa, A.; Kanno, T.; Adachi, H. Transient Response During Resistance Switching in $Ag/Pr_{0.7}Ca_{0.3}MnO_3/Pt$ Thin Films. *J. Appl. Phys.* **2006**, *99*, 016101−3.

(15) Jeon, S. H.; Park, B. H.; Lee, J.; Lee, B.; Han, S. First-Principles Modeling of Resistance Switching in Perovskite Oxide Material. *Appl. Phys. Lett.* **2006**, *89*, 042904−3.

(16) Rozenberg, M. J.; Inoue, I. H.; Sánchez, M. Nonvolatile Memory with Multilevel Switching: A Basic Model J. *Phys. Rev. Lett.* **2004**, *92*, 178302−4.

(17) Ji, L. W.; Peng, S. M.; Su, Y. K.; Young, S. J.; Wu, C. Z.; Cheng, W. B. Ultraviolet Photodetectors Based on Selectively Grown ZnO Nanorod Arrays. *Appl. Phys. Lett.* **2009**, *94*, 203106−3.

(18) Wagner, R. S.; Ellis, W. C. Vapor-Liquid-Solid Mechanism of Single Crystal Growth. *Appl. Phys. Lett.* **1964**, *4*, 89−90.

(19) Zhu, Z.; Chen, T. L.; Gu, Y.; Warren, J.; M, a. R.; Osgood, J. Zinc Oxide Nanowires Grown by Vapor-Phase Transport Using Selected Metal Catalysts: A Comparative Study. *Chem. Mater.* **2005**, *17*, 4227−4234.

(20) Lee, W.; Jeong, M. C.; Myoung, J. M. Catalyst-Free Growth of ZnO Nanowires by Metal-Organic Chemical Vapour Deposition (MOCVD) and Thermal Evaporation. *Acta Mater.* **2004**, *52*, 3949−3957.

(21) Liu, B.; Zeng, H. C. Hydrothermal Synthesis of ZnO Nanorods in the Diameter Regime of 50 nm. *J. Am. Chem. Soc.* **2003**, *125*, 4430−4431.

(22) Ohshima, E.; Ogino, H.; Niikura, I.; Maeda, K.; Sato, M.; Ito, M.; Fukuda, T. Growth of the 2-In-Size Bulk ZnO Single Crystals by the Hydrothermal Method. *J. Cryst. Growth* **2004**, *260*, 166−170.

(23) Govender, K.; Boyle, D. S.; Kenway, P. B.; O'Brien, P. Understanding the Factors that Govern the Deposition and Morphology of Thin Films of ZnO From Aqueous Solution. *J. Mater. Chem.* **2004**, *14*, 2575−2591.

(24) Yao, I. C.; Lee, D. Y.; Tseng, T. Y.; Lin, P. Fabrication and Resistive Switching Characteristics of High Compact Ga-doped ZnO Nanorod Thin Film Devices. *Nanotechnology* **2012**, *23*, 145201−8.

(25) Kind, H.; Yan, H.; Messer, B.; Law, M.; Yang, P. Nanowire Ultraviolet Photodetectors and Optical Switches. *Adv. Mater.* **2002**, *14*, 158−160.

(26) Suehiro, J.; Nakagawa, N.; Hidaka, S.; Ueda, M.; Imasaka, K.; Higashihata, M.; Okada, T.; Hara, M. Dielectrophoretic Fabrication and Characterization of a ZnO Nanowire-Based UV Photosensor. *Nanotechnology* **2006**, *17*, 2567−2573.

(27) Heo, Y. W.; Kang, B. S.; Tien, L. C.; Norton, D. P.; Ren, F.; La Roche, J. R.; Pearton, S. J. UV Photoresponse of Single ZnO Nanowires. *Appl. Phys. A* **2004**, *80*, 497−499.

(28) Francisco, H. R.; Tarancon, A.; Casals, O.; Rodriguez, J.; Albert, R. R.; Morante, J. R.; Barth, S.; Mathur, S.; Choi, T. Y.; Poulikakos, D.; Callegari, V.; Nellen, P. M. Fabrication and Electrical Characterization of Circuits Based on Individual Tin Oxide Nanowires. *Nanotechnology* **2006**, *17*, 5577−5583.

(29) Chang, W. Y.; Lai, Y. C.; Wu, T. B.; Wang, S. F.; Chen, F.; Tsai, M. J. Unipolar Resistive Switching Characteristics of ZnO Thin Films for Nonvolatile Memory Applications. *Appl. Phys. Lett.* **2008**, *92*, 022110−3.

(30) Xu, N.; Liu, L.; Sun, X.; Liu, X.; Han, D.; Wang, Y.; Han, R.; Kang, J.; Yu, B. Characteristics and Mechanism of Conduction/Set Process in TiN/ZnO/Pt Resistance Switching Random-Access Memories. *Appl. Phys. Lett.* **2008**, *92*, 232112−3.

(31) Chang, W. Y.; Lin, C. A.; He, J. H.; Wu, T. B. Resistive Switching Behaviors of ZnO Nanorod Layers. *Appl. Phys. Lett.* **2010**, *96*, 242109−3.

(32) Chiang, Y. D.; Chang, W. Y.; Ho, C. Y.; Chen, C. Y.; Ho, C. H.; Lin, S. J.; Wu, T. B.; He, J. H. Single-ZnO-Nanowire Memory. *IEEE Trans. Electr. Dev.* **2011**, *58*, 1735−1740.

(33) Yang, Y.; Zhang, X.; Gao, M.; Zeng, F.; Zhou, W.; Xie, S.; Pan, F. Nonvolatile Resistive Switching in Single Crystalline ZnO Nanowires. *Nanoscale* **2011**, *3*, 1917−1921.

(34) Ipa, K.; Thalera, G. T.; Yanga, H.; Hana, S. Y.; Lia, Y.; Nortona, D. P.; Peartona, S. J.; Jangb, S.; Ren, F. Contacts to ZnO. *J. Cryst. Growth* **2006**, *287*, 149−156.

(35) Xu, C. X.; Sun, X. W.; Zhang, X. H.; Ke, L.; Chua, S. J. Photoluminescent Properties of Copper-Doped Zinc Oxide Nanowires. *Nanotechnology* **2004**, *15*, 856−861.

(36) Lin, B.; Fu, Z.; Jia, Y. Green Luminescent Center in Undoped Zinc Oxide Films Deposited on Silicon Substrates. *Appl. Phys. Lett.* **2001**, *79*, 943−945.

(37) Yan, Y.; Tao, L. S.; Can, D.; Fei, C. P. Electronic Relaxation of Deep Bulk Trap and Interface State in ZnO Ceramics. *Chin. Phys. B* **2011**, *20*, 025201−8.

(38) Bueno, P. R.; Varela, J. A.; Longo, E. SnO_2, ZnO and Related Polycrystalline Compound Semiconductors: An Overview and Review on the Voltage-Dependent Resistance (Non-Ohmic) Feature. *J. Eur. Ceram. Soc.* **2008**, *28*, 505−529.

(39) Yuk, J. M.; Kim, K.; Lee, Z.; Watanabe, M.; Zettl, A.; Kim, T. W.; No, Y. S.; Choi, W. K.; Lee, J. Y. Direct Fabrication of Zero- and One-Dimensional Metal Nanocrystals by Thermally Assisted Electromigration. *ACS Nano* **2010**, *4*, 2999−3004.

(40) Zhang, J.; Yang, H.; Zhang, Q. l.; Dong, S.; Luo, J. K. Bipolar Resistive Switching Characteristics of Low Temperature Grown ZnO Thin Films by Plasma-Enhanced Atomic Layer Deposition. *Appl. Phys. Lett.* **2013**, *102*, 012113−4.

(41) Guan, W.; Liu, M.; Long, S.; Liu, Q.; Wang, W. On the Resistive Switching Mechanisms of Cu/ZrO_2 : Cu/Pt. *Appl. Phys. Lett.* **2008**, *93*, 223506−3.

(42) Park, G.S; Li, X. S.; Kim, D. C.; Jung, R. J.; Lee, M. J.; Seo, S. Observation of Electric-Field Induced Ni Filament Channels in Polycrystalline NiO_x Film. *Appl. Phys. Lett.* **2007**, *91*, 222103−3.

(43) Shi, W.; Tai, Q..; Xia, X. H.; Yi, M. D.; Xie, L. H.; Fan, Q. L.; Wang, L. H.; Wei, A.; Huang, W. Unipolar Resistive Switching Effects Based on Al/ZnO/P^{++}-Si Diodes for Nonvolatile Memory Applications. *Chin. Phys. Lett.* **2012**, *29*, 087201−4.

(44) Wong, H. S. P.; Lee, H. Y.; Yu, S.; Chen, Y. S.; Wu, Y.; Chen, P. S.; Lee, B.; Chen, F. T.; Tsai, M. Metal−Oxide RRAM. *Proc. IEEE* **2012**, *100*, 1951−1970.

(45) Kwon, D. H.; Kim, K. M.; Jang, J. H.; Jeon, J. M.; Lee, M. H.; Kim, G. H.; Li, X. S.; Park, G. S.; Lee, B.; Han, S.; Kim, M.; Hwang, C. S. Atomic Structure of Conducting Nanofilaments in TiO_2 Resistive Switching Memory. *Nat. Nanotechnol.* **2010**, *5*, 148−153.

(46) Son, D. I.; Kim, T. W.; Shim, J. H.; Jung, J. H.; Lee, D. U.; Lee, J. M.; Park, W.I.; Choi, W. K. Flexible Organic Bistable Devices Based on Graphene Embedded in an Insulating Poly(methyl methacrylate) Polymer Layer. *Nano Lett.* **2010**, *10*, 2441−2447.

(47) Pagina, H.; Sotnik, N. Bistable Switching in Electroformed Metal-Insulator-Metal Devices. *Phys. Stat. Sol. A.* **1988**, *108*, 11−65.